Sensors and Materials, Vol. 38, No. 8 (2026) 4919–4936
MYU Tokyo

S & M 4602

Prediction of Initial Wave Amplitude Induced by Submarine Landslides Using Smoothed Particle Hydrodynamics

Hyeon-Jeong Kim,* Ji Yoon Kim, Yoomi Choi, and Byung-Il Min

Department of Environmental and Disaster Assessment Research Division,
Korea Atomic Energy Research Institute,
111, Daedeok-daero 989 beon-gil, Yuseng-gu, Daejeon 34057, Republic of Korea

(Received December 3, 2025; accepted August 13, 2026)

Keywords: submarine landslide, tsunami, landslide-generated waves, smoothed particle hydrodynamics

In this study, we focused on developing a new equation for predicting the initial wave amplitude induced by submarine landslides, based on a smoothed particle hydrodynamics (SPH) model that considers fluid–rigid body interactions. Existing empirical equations were primarily derived from wave flume experiments conducted under limited landslide parameter conditions, which limit their applicability to extended scenarios. To overcome these limitations, a range of landslide parameters was systematically established and replicated through numerical modeling. The water surface response within the simulation was quantified using a numerical sensing approach. The simulated water surface elevations were compared with laboratory wave-gauge measurements with high accuracy, demonstrating sufficient predictive accuracy to complement laboratory experiments. Furthermore, the relationship between major landslide parameters and initial wave amplitude was nondimensionalized and a new equation was derived through log-linear regression analysis. The proposed equation was able to predict initial wave amplitudes observed in both laboratory and field settings, confirming its applicability in the field. These results suggest that the developed equations can be applied to early tsunami risk assessment and early warning systems in coastal areas vulnerable to submarine landslide tsunamis.

1. Introduction

Submarine landslides are a potential natural hazard capable of triggering large-scale tsunamis, posing a serious threat to major coastal infrastructure developed as strategic national hubs and densely populated communities. The tsunami that struck Papua New Guinea on July 17, 1998, is recognized as a significant event because it demonstrated that small and relatively submarine mass failure (SMF) can cause devastating local tsunamis that strike without warning.(1) A recent representative case is the Mw 7.5 earthquake that struck Indonesia, Central Sulawesi, on September 28, 2018. This earthquake occurred offshore, followed by a coastal landslide and destructive tsunami waves that occurred in succession in Palu Bay. A maximum

*Corresponding author: e-mail: liswjd@gmail.com
https://doi.org/10.18494/SAM6201

ISSN 0914-4935
https://myukk.org/

run-up of 10.5 m was observed in the southeastern part of Palu Bay, causing numerous casualties and significant coastal damage.(2) As such, SMF occurs at a very close distance to the coast and exhibits the characteristic of generating relatively high tsunami waves despite the earthquake's magnitude, reaching the coast within a short time.

Research(3) was conducted to understand the tsunami phenomenon in the aforementioned situation and to elucidate its generation mechanism. In the initial study, experiments were performed in a wave flume, distinguishing the landslide geometry into solid blocks and granular material, to observe their behavior on an inclined surface. Landslides composed of granular material generated relatively smaller wave amplitudes than solid blocks under identical geometric and kinematic conditions. These results indicate that the water displacement generated by solid blocks provides an upper bound on the wave amplitude that an actual deformable landslide may induce.(3) Furthermore, major parameters affecting surface displacement by solid blocks (e.g., initial acceleration, center of mass motion, and added mass coefficient) were presented. Subsequent submarine landslide studies(4–6) primarily employed hydraulic model experiments using rigid bodies, and the obtained results serve as validation data for various numerical models.

Studies have been conducted to reproduce the motion characteristics, initial wave amplitude, and waveform of SMF derived from various wave flume experiments into numerical models.(7–11) In previous studies, the approximate equation of motion describing the center of mass displacement of rigid underwater landslides was used as the boundary condition of the numerical model, and the water surface displacement caused by SMF was successfully simulated using the boundary element method and fully nonlinear potential flow.

Smoothed particle hydrodynamics (SPH) is considered a suitable method for simulating free-surface fluctuations caused by landslides, as it can directly calculate the interaction between fluids and rigid bodies using a Lagrangian approach.(12,13) SPH is particularly flexible in handling complex boundary conditions and abrupt topographic changes, offering the advantage of precisely simulating submarine slope failures and the initial tsunami formation process. However, SPH numerical analysis requires high computational costs, limiting its use as an immediate prediction tool at field scale.

Furthermore, research(5,11) on developing predictive equations for estimating the maximum initial wave amplitude of submarine landslides has also been continuously conducted. Scaling-based approaches for estimating initial wave amplitude have been widely utilized in numerous previous studies.(3,5) These studies commonly reduce major variables to dimensionless numbers and derive regression equations by assuming a power-law relationship between tsunami amplitude and slope conditions. These empirical equations are derived by considering parameters related to landslides based on previously limited wave flume experiments. However, they have limitations in securing generalized prediction performance for diverse landslide scenarios owing to their narrow applicability range (e.g., slope angle and SMF density).

In this study, we propose a new prediction formula that can rapidly estimate the initial wave amplitude of a landslide tsunami. To achieve this, we verify the validity and effectiveness of the SPH model to precisely reproduce wave flume experiments. The water surface response induced by SMF was quantified using a numerical sensing approach within the SPH model and compared with water-level measurements obtained using wave gauges in laboratory experiments. Furthermore, we extend the application of major landslide parameters and derive correlations with initial wave amplitude. We then examine the applicability of the new prediction formula to field applications.

2. Methods

The fundamental theory and detailed algorithms of the SPH model are sufficiently presented in existing literature.(14–17) Therefore, in this section, we briefly introduce only the major elements necessary for analyzing the submarine landslide problem. Subsequently, we sequentially describe the verification using existing wave flume experiments,(3) the configuration of numerical experiments for new experimental conditions, and the procedure for constructing a regression model for tsunami amplitude prediction.

2.1 Numerical model

2.1.1 DualSPHysics

In this study, we employed DualSPHysics Ver. 5.2,(15) based on the SPH method, to simulate water surface displacement caused by SMF. DualSPHysics is available as open-source software and can perform numerical calculations using both CPU and GPU processors. It can also be used to analyze problems such as dam failures and wave–structure interaction. While traditional Eulerian grid-based methods have limitations in handling large deformations or free surfaces, SPH employs a mesh-free Lagrangian approach, representing the fluid as a collection of discrete particles, each carrying state variables such as mass, density, velocity, and pressure. These characteristics make SPH highly suitable for simulating nonlinear surface displacements such as those in landslide-generated waves and fluid–rigid body interactions.

The governing equations for SPH include the continuity and momentum equations, which ensure mass and momentum conservation. The continuity equation is expressed as

$$\frac{d\rho_a}{dt} = \sum_b m_b \left(\boldsymbol{v}_a - \boldsymbol{v}_b\right) \cdot \nabla W_{ab}\left(h\right), \tag{1}$$

where ρ_a is the density of particle a, v_a and v_b are the velocities of particles a and b, respectively, m_b is the mass of particle b, and $W_{ab}(h)$ is the kernel function that interpolates between neighboring particles.(18) The smoothing length h controls the radius within which neighboring particles affect each other.

The momentum equation governs the forces acting on particles, including pressure and viscous effects:

$$\frac{d\boldsymbol{v}_a}{dt} = -\sum_b m_b \left(\frac{P_a}{\rho_a^2} + \frac{P_b}{\rho_b^2} + \Pi_{ab} \right) \nabla W_{ab}(h) + g , \tag{2}$$

where P_a and P_b represent pressures, ρ_a and ρ_b are densities, and Π_{ab} accounts for artificial viscosity to stabilize the momentum equation, particularly under strong compression.[19]

2.1.2 CHRONO engine coupling

In this study, DualSPHysics was coupled with the multiphysics simulation engine CHRONO to accurately reproduce the motion of a solid block sliding down a slope and to precisely calculate fluid–rigid body interaction. CHRONO is a high-performance dynamics solver capable of calculating complex contact, collision, friction, and structural dynamics.

In the submarine landslide problem, the solid block initially exists in contact with the slope surface. It then begins to move as it accelerates under the effects of gravity and fluid forces. Subsequently, it slides along the slope, displacing the surrounding fluid and causing surface water fluctuations. To accurately handle collisions and friction between the rigid body and the slope boundary, as well as pressure and viscous forces between the rigid body and the fluid during this process, CHRONO's rigid-body solver is utilized.

The DualSPHysics–CHRONO coupling is implemented using a message-passing approach. First, DualSPHysics calculates the interactions between fluid particles and the pressure and viscous forces between the fluid and the rigid body. At each time interval Δt, the fluid forces acting on the rigid body and the resulting angular momentum changes are communicated to CHRONO. CHRONO uses these data to calculate the rigid body's new velocities and positions. The rigid body information computed by CHRONO is then passed back to DualSPHysics, updating the positions and velocities of the rigid-body particles, and the entire fluid–rigid body system advances to the $t + \Delta t$ step.

The temporal coupling is configured so that DualSPHysics and CHRONO share the same time step, enabling complete interaction modeling without predefining rigid body motion under specific kinematic conditions. This allows the real-time exchange of mechanical properties such as rigid body slippage, collision, rotation, and rebound, along with changes in fluid forces, thereby reproducing the actual behavior of submarine landslides.

2.2 Numerical setup

2.2.1 Computational domain and boundary conditions

Actual SMF may occur in various forms, including granular and block-like failures. However, previous laboratory and numerical studies[3,6,7,10,11] have commonly idealized SMF as a rigid body to investigate the fundamental wave-generation mechanism. These studies have shown that the initial wave amplitude is primarily governed by the center-of-mass motion and initial acceleration of the sliding mass. In addition, granular landslides tend to generate smaller initial wave amplitudes than rigid landslides because part of their energy is dissipated through shape deformation and mass spreading during motion.[3,10] Therefore, in this study, SMF was assumed to be a triangular rigid body, and numerical simulations were performed to reproduce the dominant kinematic characteristics governing the initial wave amplitude.

The numerical simulation domain was configured as shown in Fig. 1, referencing the indoor wave flume experimental conditions performed in previous studies.[3] The total length of the flume was set to 9.14 m, and the still water depth was adjusted according to each experimental condition. The computational domain was defined in two dimensions for comparison with existing physical model experiments.

The solid block simulating SMF was modeled as an isosceles triangle and initially placed in contact with the slope. The initial particle spacing between fluid and boundary particles within the computational domain was set to d_p = 0.0001 m. Accordingly, approximately 3.18×10^6 particles were distributed throughout the entire computational domain, with boundaries consisting of about 1.28×10^6 particles.

The dynamic boundary condition method was applied to all fixed boundaries, such as the bottom, side walls, and inclined surfaces of the tank, to stably simulate fluid–boundary interactions.[20] This method effectively suppresses pressure oscillations near the boundary and provides physically consistent conditions to prevent free-surface flow from passing through the boundary.

The SMF solid block was input as a stereo lithography shape, and the rigid body density was defined according to each experimental condition. The motion of the collapsing body was calculated using Project Chrono, accounting for kinetic friction with the slope (k_{fric} = 0.0006), the coefficient of restitution upon collision (e = 0.85), and the effects of pressure and viscous forces exerted by the fluid. These settings ensured that the collapsing body was accelerated by gravity and fluid forces, sliding down the slope and displacing the surrounding fluid through a physically natural process.

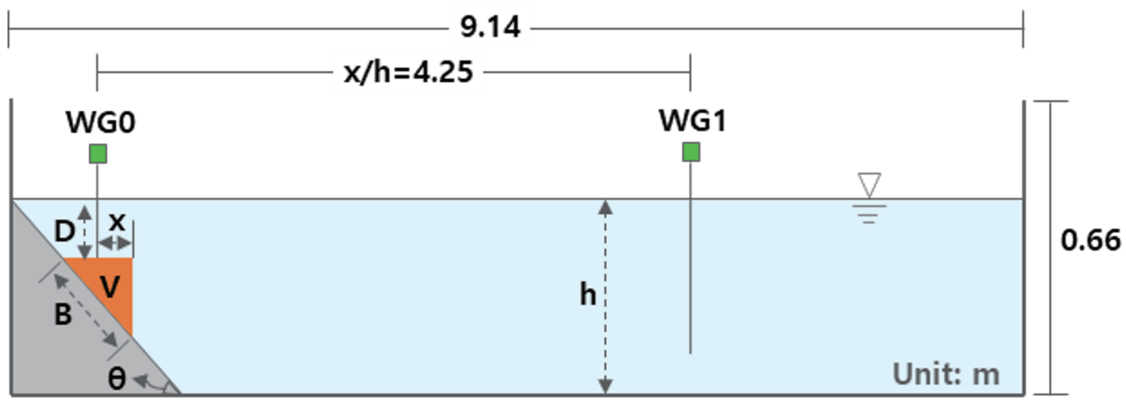

Fig. 1. (Color online) Conceptual diagram for simulating a submarine landslide in a wave flume.

This numerical calculation domain and boundary condition setting served as the basis for the consistent analysis of the initial water surface displacement characteristics occurring under various slope failure conditions, as well as for quantitative comparison with wave flume experiments.

2.2.2 Submarine landslide parameters

The configuration of landslide parameters is broadly divided into two stages. The first stage, aimed at validating the numerical model, reorganized the parameter characteristics (e.g., V and B) and the density of the solid block based on the experimental conditions conducted in a previous study(3) and presented in Table 1. These conditions were used to verify whether the DualSPHysics model adequately reproduces submarine landslide phenomena in a wave flume, as shown in Fig. 1. A total of 43 configurations were created, each differing based on the parameters, allowing the observed waveforms to be directly compared with the numerical simulations.

Second, we newly defined landslide parameters to develop a scaling law equation capable of predicting initial wave amplitude. Since previous experiments were conducted only within limited parameter ranges, we systematically varied major parameters: solid block volume (V), block length (B), initial submergence depth (D), density (ρ), and slope angle (θ) to establish new parameters (Table 2). In Run-B, 11 combinations of slide block length variations were set; in

Table 1
Parameters of the solid block used to reproduce a submarine landslide.

Tag	Block #	V (10^{-3} m^3)	B (m)	D (m)	ρ (kg/m^3)	h (m)
1N	43, 44, 61, 65, 77, 78	7.744	0.175	0.045−0.074	1890	0.368, 0.373
2A	28, 69	3.630	0.122	0.075	1460	0.373
2B	29, 70	3.630	0.122	0.075	1710	0.373
2C	30, 71	3.630	0.122	0.075	2180	0.373
2D	48, 74	3.630	0.122	0.073–0.075	2180	0.373
2E	31, 49, 72, 75	3.630	0.122	0.073–0.075	2465	0.373
2L	42, 73	3.630	0.122	0.074−0.075	2745	0.373
2N	25, 26, 27, 47, 52, 56, 57, 60, 62, 66, 67, 79	3.630	0.122	0.040−0.116	1870	0.373
2O	41, 68	3.630	0.122	0.074–0.075	1225	0.373
3N	51, 55, 58, 59, 63, 64, 76, 80	1.871	0.086	0.052−0.105	1835	0.373, 0.406
4N	50	0.784	0.057	0.085	1835	0.416

*Landslide parameters were rearranged on the basis of the experimental specifications proposed in a previous study.(3)

Table 2
Landslide parameters for simulating various solid block conditions.

Tag	V (10^{-3} m^3)	B (m)	D (m)	ρ (kg/m^3)	θ (°)	h (m)
Run-B	1.406–12.656	0.075–0.225	0.150	2000	45	0.5
Run-AD	5.625	0.150	0.004−0.285	2000	22.5, 45.0, 67.5	0.5
Run-R	5.625	0.150	0.150	1400–2800	45	0.5

Run-AD, 58 combinations of varying slope angles and initial submergence depths were considered; and in Run-R, 15 combinations of block density variations were applied, resulting in a total of 84 cases. These parameters encompass a wider range of conditions than those addressed in previous experimental studies and are utilized to derive a predictive relationship for the initial wave amplitude generated by SMF.

2.3 Tsunami amplitude fitting procedure

In this study, we analyzed the relationship between the main parameters of landslides and the initial wave amplitude based on numerical model results under a wider range of conditions than in previous studies.(3,5) To this end, the fitting process is described in detail. Specifically, the combination of dimensionless numbers, log-linearization, the inclusion of interaction and quadratic terms, and the regression coefficient estimation procedure using Huber robust regression are presented step-by-step.

2.3.1 Construction of scaling-based prediction model

In this study, a dimensionless scaling approach was applied to predict the initial depression tsunami amplitude generated by submarine landslides. First, the governing variables were expressed as dimensionless numbers according to Buckingham, and the dimensionless numbers used are as follows.

$$\Pi_V = \frac{V}{BD^2},\ \Pi_B = \frac{D}{B},\ \Pi_R = \frac{\rho_s}{\rho_w},\ S = \sin\theta. \tag{3}$$

Here, V is the volume of the solid block (m^3), B is the length of the block in contact with the slope (m), D is the initial submergence depth (m), ρ_s is the density of the solid block, ρ_w is the density of water (kg/m^3), and θ is the slope angle. The dependent variable was defined as follows after being made dimensionless.

$$\eta_B = \frac{\eta_{max}}{B} \tag{4}$$

Here, η_{max} is defined as the initial wave amplitude by the block length, representing the dimensionless tsunami amplitude.

2.3.2 Log-transformed regression model

Previous studies(3) presented correlations with parameters significantly affecting tsunami amplitude in a power-law form, and these correlations were referenced. In this study, a log transformation was applied to all variables to convert them into a form suitable for linear regression. This transformation has the advantage of converting the power law into a linear form, stabilizing variance and reducing the effect of outliers.

$$y = \log_{10}\left(\eta_B\right) \tag{5}$$

$$x_1 = \log_{10}(\Pi_V),\ \ x_2 = \log_{10}(\Pi_B),\ \ x_3 = \log_{10}(S),\ \ x_4 = \log_{10}(\Pi_R) \tag{6}$$

In this study, considering the analysis and existing prior research,[3,5] the following extended log-linear equation was adopted as the regression model.

$$y = \beta_0 + \beta_1 x_1 + \beta_2 x_2 + \beta_3 x_3 + \beta_4 x_4 + \beta_5 x_1^2 + \beta_6 x_1 x_3 + \varepsilon \tag{7}$$

Here, the term x_1^2 reflects the nonlinear effect of the dimensionless number Π_V (related to volume and submergence depth), whereas the term $x_1 x_3$ is appropriately selected to improve the predictive accuracy of the regression equation. ε is the residual error term, representing the difference between the input and predicted values, and is treated as a linear loss to mitigate the effect of outliers.

2.3.3 Regression and model evaluation

To minimize the effects of data dispersion heterogeneity and outliers, we applied a robust linear model using the Huber loss function. The Huber loss has the advantage of mitigating the impact of outliers by applying a quadratic loss to small residuals and a linear loss to large residuals, thereby ensuring the stability and robustness of the linear regression. Regression was performed using the robust linear model function from Python's statsmodels package, with all variables input as dimensionless and log-transformed values.

The optimal regression coefficients (β_i) obtained by fitting the numerical simulation results were used to predict η_{max} from the landslide parameters of the experimental cases reported in previous studies. The model's predictive performance is evaluated using the coefficient of determination (R^2), root mean squared error ($RMSE$), and normalized root mean squared error ($NRMSE$), for both the entire dataset and subsets. Additionally, the regression model's fit and reliability were verified by visualizing the prediction-experimental scatter plot and the ±10 or ±20% relative error interval. Each error is defined as follows.

$$R^2 = 1 - \frac{\sum_{i=1}^{n}\left(Obs_i - Cal_i\right)^2}{\sum_{i=1}^{n}\left(Obs_i - \overline{Obs}\right)^2} \tag{8}$$

$$RMSE = \sqrt{\frac{1}{n}\sum_{i=1}^{n}\left(Obs_i - Cal_i\right)^2} \tag{9}$$

$$NRMSE = \frac{\sqrt{\sum_{i=1}^{n}\left(Obs_i - Cal_i\right)^2}}{\sqrt{\sum_{i=1}^{n}\left(Obs_i - \overline{Obs}\right)^2}} \tag{10}$$

Here, Obs_i and Cal_i represent the observed and predicted values, respectively, and $\overline{Obs}$ is the average of the observed values.

3. Results

3.1 SPH model validation

We reproduced the phenomenon of a solid block moving along a landslide slope in a wave flume to validate the DualSPHysics model. Various solid block conditions presented in Table 1 were applied, and water level changes were analyzed for a total of 43 variations in major landslide parameters: density, initial submergence depth, and solid block length. The reference point is WG0 (wave gauge) shown in Fig. 1, and the time-varying water surface elevation calculated at the top center of the solid block was compared. Figure 2 shows 12 results that are most representative of the characteristics of the landslide parameter variations, confirming that this model can effectively reproduce SMF.

The verification results for density variation (Fig. 2, left panel) clearly demonstrate the characteristic that blocks with the same volume but increased weight induce a larger initial depression. Water surface elevation follows a trend highly consistent with the experimental data, showing a greater drop and rise for blocks with higher density. The timing of maximum depression and the phase of the waveform show results very close to the experimental values.

The reproducibility of this model was also confirmed in comparisons based on changes in initial submergence depth (Fig. 2, middle panel). As the block's submergence depth decreases, the effect on the fluid surface increases, and this was stably and accurately reproduced in the numerical model. This demonstrates that the SPH model appropriately simulates the pressure and momentum resulting from fluid–rigid body interaction.

Finally, a high degree of agreement between the model and experimental results was also confirmed in the comparison of solid block length changes (Fig. 2, right panel). In the experimental case, as the length increases, the volume of SMF can be seen to increase, leading to larger displacement scales and causing greater fluctuations in water surface elevation. This confirms that the model exhibits sufficient sensitivity to changes in block geometry.

The results of 43 numerical simulations were compared in Fig. 3 by correlating the maximum depression values at η_{max}. The observed and calculated values are generally distributed evenly around a reference line with a slope of 1, confirming that the numerical model quantitatively reproduces the initial wave amplitude well. The relative error ranges of ±10 and ±20% are indicated by gray and red shading, respectively. Most comparison points fall within ±20%, and a significant number are within ±10%, demonstrating the numerical model's high predictive

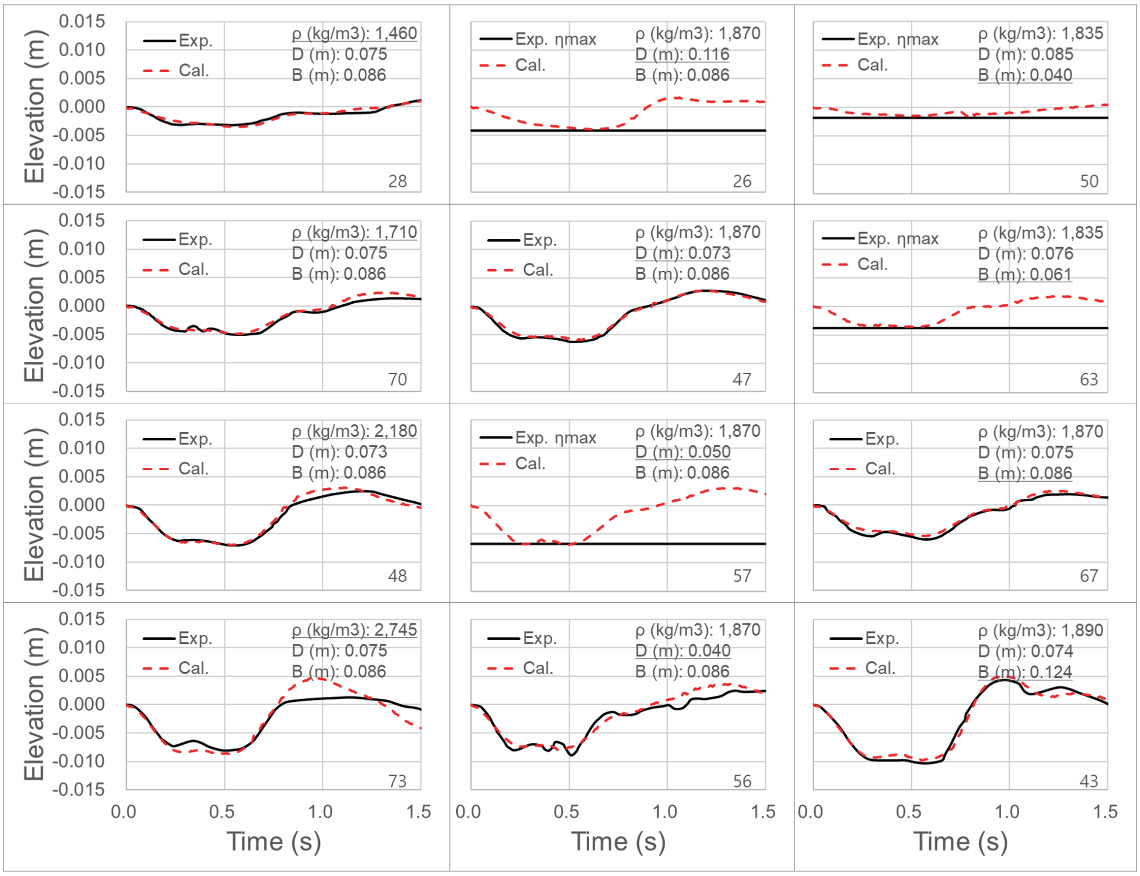

Fig. 2. (Color online) Comparison of numerical simulation results (Cal.) with the water surface elevation measurements (Exp.) reported.(3) The left, middle, and right panels illustrate the effects of varying solid-block density (ρ), initial submergence depth (D), and slide-block length (B), respectively.

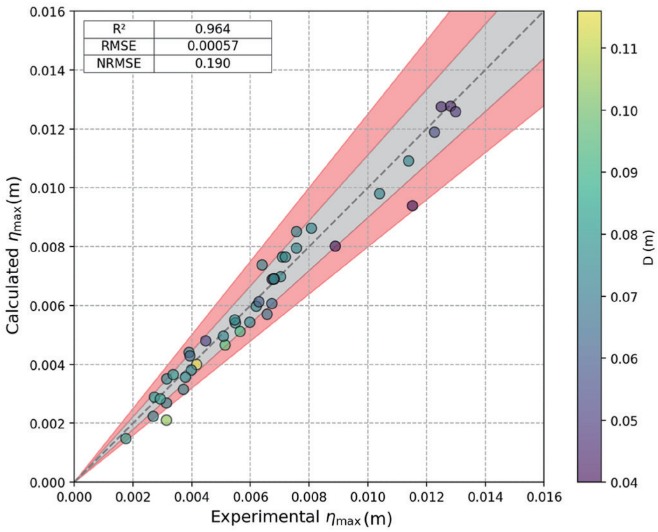

Fig. 3. (Color online) Comparison between calculated and experimental initial wave amplitude (η_{max}) values. The relative error bands are colored gray (±10%) and red (±20%), and the color of the circular symbol represents the initial submergence (D) value of the solid block.

performance. The color scale represents the initial submergence depth (D) of the solid block. The experimental trend showing an increase in η_{max} with decreasing submergence depth is partially reflected in the numerical simulation. Statistically, high consistency is also observed, with R^2 calculated as 0.964, *RMSE* as 5.7×10^{-4} m, and *NRMSE* as 0.19.

3.2 Landslide parameter analysis

The characteristics of the initial wave amplitude were analyzed on the basis of the major landslide parameters: block volume, length, initial submergence depth, density, and slope angle. Figure 4 shows the power-law correlations for each parameter by plotting the numerical simulation results alongside existing experimental observations.[3,6] Additionally, Table 3

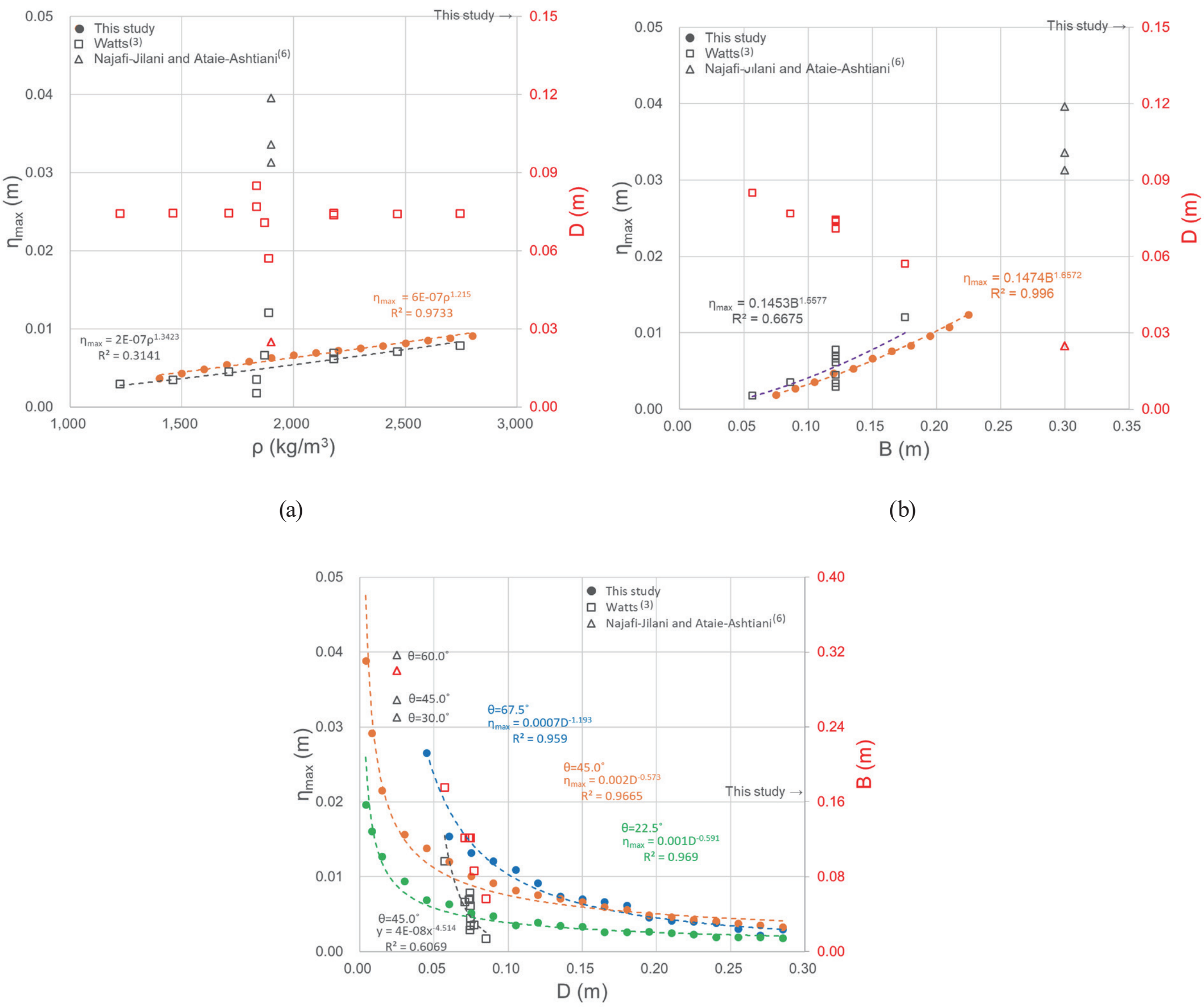

(c)

Fig. 4. (Color online) Power-law relationships between η_{max} and major landslide parameters: (a) solid-block density (ρ), with the corresponding initial submergence depth (D) plotted on the secondary axis; (b) slide-block length (B), with the associated D–B relationship on the secondary axis; and (c) initial submergence depth (D) for various slope angles (θ), with the slide-block length (B)–D relationship shown on the secondary axis.

Table 3
Results of η_{max} sensitivity analysis according to variations in landslide parameters (B, D, and ρ).

Landslide parameter condition according to relative change				Calculated η_{max} (10^{-2} m) and relative rate (%)		
Relative rate (%)	Run-B B (m)	Run-AD$_{45°}$ D (m)	Run-R ρ (kg/m^3)	B	D	ρ
−97		0.004			3.886 (485.0)	
−95		0.008			2.920 (339.6)	
−90		0.015			2.153 (224.0)	
−80		0.030			1.563 (135.3)	
−70		0.045			1.380 (107.7)	
−60		0.060			1.205 (81.4)	
−50	0.075	0.075		0.189 (−71.6)	1.009 (51.9)	
−40	0.090	0.090		0.274 (−58.8)	0.915 (37.8)	
−30	0.105	0.105	1400	0.358 (−46.1)	0.819 (23.3)	0.368 (−44.6)
−20	0.120	0.120	1600	0.471 (−29.1)	0.757 (13.9)	0.485 (−27.0)
−10	0.135	0.135	1800	0.531 (−20.0)	0.709 (6.7)	0.583 (−12.2)
0	0.150	0.150	2000	0.664	0.664	0.664
10	0.165	0.165	2200	0.760 (14.4)	0.597 (−10.1)	0.722 (8.6)
20	0.180	0.180	2400	0.833 (25.5)	0.563 (−15.2)	0.784 (18.0)
30	0.195	0.195	2600	0.962 (44.8)	0.489 (−26.4)	0.850 (27.9)
40	0.210	0.210	2800	1.077 (62.2)	0.463 (−30.3)	0.909 (36.8)
50	0.225	0.225		1.237 (86.3)	0.429 (−35.7)	
60		0.240			0.409 (−38.5)	
70		0.255			0.378 (−43.1)	
80		0.270			0.355 (−46.5)	
90		0.285			0.331 (−50.1)	

quantitatively presents the increase or decrease in initial submergence depth when each variable is varied by ±10% relative to the reference conditions (B = 0.15 m, D = 0.15, and ρ = 2000 kg/m^3). The initial submergence depth was increased by a maximum of −95 or −97%, and the slope angle is based on 45°.

Density exhibits a gradual curve-shaped change in its correlation with η_{max}, showing a characteristic where the decrease in η_{max} is more pronounced when density decreases rather than increases. Block length shows a symmetrical change rate from −46 to 45%. However, overall regression tends to follow a power-law pattern. Conversely, changes in initial submergence depth exhibit an inverse relationship with η_{max}. Around 0.05 m, η_{max} increases sharply in an exponential form. Additionally, slope angles were categorized into three types (22.5, 45, and 67.5°) to analyze the corresponding variations in η_{max}. Generally, as slope angle increases, η_{max} shows an overall increasing trend.

3.3 Predictive equation for initial wave amplitude

Regression was performed using a total of 84 datasets, from which the coefficient values for the final prediction equation [Eq. (7)] regarding the dimensionless initial wave height (η_{max}/B) were derived (Table 4). The regression dataset covered landslide densities of 1400–2800 kg/m^3, slope angles of 22.5, 45.0, and 67.5°, block lengths of 0.075–0.225 m, and submergence depths of 0.004–0.285 m. This prediction equation did not directly incorporate power laws derived from

Table 4
Coefficient value of the optimized regression equation.

β_0	β_1	β_2	β_3	β_4	β_5	β_6
1.07	0.237	−0.425	0.978	1.245	−0.0538	0.048

existing observational data (e.g., $\eta_{max} \propto \rho^{1.215}$ and $\eta_{max} \propto B^{1.657}$). Instead, it adopted a log-linear form based on a dimensionless dataset that sufficiently captured these trends to derive the optimal fitting equation.

The calculated η_{max} and η_{max}/B values derived from the prediction equation are presented in Fig. 5 for comparison with the experimental values. The log-transformed dimensionless η_{max}/B shown in Fig. 5(a) indicates that, except for the condition with a slope angle of 67.5°, the *NRMSE* ranges from 0.097 to 0.282 across the entire dataset, whereas the 67.5° slope condition shows a somewhat higher *NRMSE* of 0.515. Furthermore, the dimensionless η_{max}/B and η_{max} values presented in Figs. 5(b) and 5(c) mostly fall within a relative error of ±10%.

Figure 5(d) compares the prediction accuracy of the proposed prediction equation with that of the prediction equation proposed in a previous study.(5) The *NRMSE* for the block length, slope angle, and density cases decreased from 0.42 to 0.13, from 1.44–53.15 to 0.09–0.31, and from 1.60 to 0.23, respectively.

The landslide parameters used in the wave flume experiments are summarized in Table 5. Comparison of the predicted and experimental η_{max} values showed relative errors ranging from −23.3 to 22.5%, with an R^2 of 0.94.

4. Discussion

In this study, we simulated the interaction between a solid block and a fluid using numerical simulations combining DualSPHysics and CHRONO. Specifically, the motion of the solid block was naturally modeled by the block's physical properties (e.g., density and volume) and external forces (e.g., gravity and drag force), without requiring separate consideration of empirical coefficients such as initial acceleration or additional mass coefficients derived from wave flume experiments. This demonstrates that the proposed numerical model can physically simulate the fundamental dynamics of SMF.

The numerical simulation results showed that a depression formed at the still water surface as the solid block descended along the slope, and the waveform closely matched the wave flume experimental results. In particular, the initial wave amplitude exhibiting the maximum depression showed a high correlation (R^2 = 0.964), confirming that the proposed model can quantitatively reproduce the initial wave amplitude in SMF.

The expanded analysis of major landslide parameters in this study revealed an exponential increase in the initial wave amplitude when the initial submergence depth was less than approximately 0.05 m. This is interpreted as a result of the potential energy change due to SMF movement being more directly transferred to the water surface at smaller submergence depths. When the distance between the water surface and the block is sufficiently large, the water above the block acts as a buffer, reducing water surface deformation. However, at very small

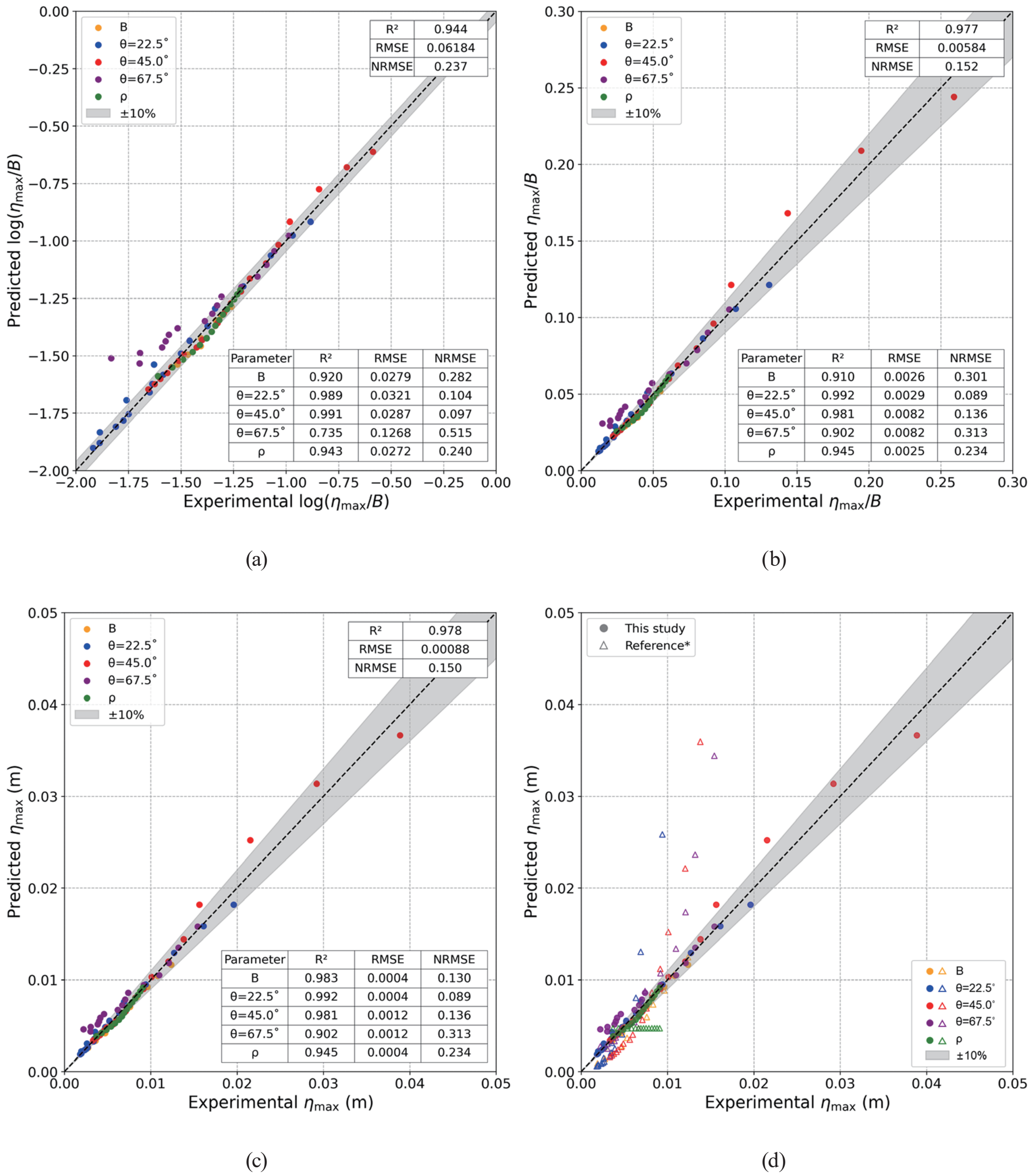

Fig. 5. (Color online) The initial wave amplitude predicted using a regression equation was compared with data from a wave flume experiment. (a) is the log-scale, nondimensionalized η_{max}/B, (b) is the nondimensionalized η_{max}/B, (c) is η_{max}, and (d) is the result of an empirical equation presented in a previous study.(5)

submergence depths, the spatial changes in SMF are assumed to directly lead to surface lowering. This nonlinear response has not been sufficiently elucidated in previous experimental studies, and future, intensive wave flume experiments across the relevant depth range are needed to more clearly elucidate the physical mechanisms. However, the prediction equation presented in this study reflects these characteristics, making it significant in that it expands the scope of predictive applicability.

Table 5
Comparison of experimental and calculated initial wave amplitudes (η_{max}) and non-dimensional amplitudes (η_{max}/B) for various landslide block configurations.

Tag	V (m^3)	B (m)	D (m)	ρ (kg/m^3)	θ (°)	Experimental		Calculated		Relative error (%)
						η_{max} (m)	η_{max}/B	η_{max} (m)	η_{max}/B	η_{max}
N1	7.744×10^{-3}	0.175	0.057	1890	45	1.206×10^{-2}	0.069	1.122×10^{-2}	0.064	−7.0
A2	3.630×10^{-3}	0.122	0.075	1460	45	0.334×10^{-2}	0.028	0.383×10^{-2}	0.031	14.7
B2	3.630×10^{-3}	0.122	0.075	1710	45	0.450×10^{-2}	0.037	0.466×10^{-2}	0.038	3.6
C2	3.630×10^{-3}	0.122	0.075	2180	45	0.615×10^{-2}	0.051	0.631×10^{-2}	0.052	2.6
D2	3.630×10^{-3}	0.122	0.074	2180	45	0.691×10^{-2}	0.057	0.636×10^{-2}	0.052	−8.0
E2	3.630×10^{-3}	0.122	0.074	2465	45	0.706×10^{-2}	0.058	0.738×10^{-2}	0.061	4.5
L2	3.630×10^{-3}	0.122	0.074	2745	45	0.783×10^{-2}	0.064	0.843×10^{-2}	0.069	7.7
N2	3.630×10^{-3}	0.122	0.071	1870	45	0.661×10^{-2}	0.054	0.541×10^{-2}	0.044	−18.2
O2	3.630×10^{-3}	0.122	0.074	1225	45	0.292×10^{-2}	0.024	0.309×10^{-2}	0.025	5.8
N3	1.871×10^{-3}	0.086	0.077	1835	45	0.355×10^{-2}	0.041	0.290×10^{-2}	0.034	−18.3
N4	0.784×10^{-3}	0.057	0.085	1835	45	0.176×10^{-2}	0.031	0.135×10^{-2}	0.024	−23.3
T4	1.95×10^{-2}	0.040	0.025	1900	30	3.130×10^{-2}	0.104	2.688×10^{-2}	0.090	−14.1
T13	1.95×10^{-2}	0.040	0.025	1900	45	3.360×10^{-2}	0.112	3.902×10^{-2}	0.130	16.1
T10	1.95×10^{-2}	0.040	0.025	1900	60	3.960×10^{-2}	0.132	4.852×10^{-2}	0.162	22.5

*Landslide parameters used in wave flume experiments and observed η_max in previous studies.[3,6]

Furthermore, on the basis of numerical simulations conducted under various conditions, a new prediction equation was proposed to elucidate the relationship between initial wave amplitude and major landslide parameters. To evaluate the field applicability of the proposed prediction equation, a comparison was conducted with the 2018 Palu Bay tsunami case reported in previous studies.[2,21] In this study, water surface elevation was indirectly estimated through video monitoring, and major parameters of the submarine landslide, such as the start position, slope angle, and sliding length, were estimated using high-resolution bathymetry data. The major landslide parameters and depressed maximum wave amplitudes derived from these data are presented in Table 6, and a comparison with the prediction equation results is shown in Fig. 6.

The comparison results show that while the laboratory scale used to simulate SMF exhibited a relative error of approximately ±20%, the field scale showed −10% for R1 and approximately twice as large for R2, indicating a difference depending on the location of occurrence. These differences are attributed to the difference in distance between the video monitoring points observed in the field and the actual location of SMF occurrence, as well as uncertainties in the landslide parameter estimation process. Furthermore, in actual sea areas, surface displacements can be more complex than the simplified conditions assumed in this study owing to spatially changing seafloor topography and progressive or multiple landslide processes that may occur after an earthquake, and it is determined that these factors acted as causes of prediction errors.

The prediction equation proposed in the previous study[5] was derived from hydraulic experiments using a solid block with a single density (2600 kg/m^3) and therefore could not account for the effect of varying landslide densities. In contrast, the proposed prediction equation was developed using numerical simulation results for landslide densities ranging from 1400 to 2800 kg/m^3, allowing the effect of density on the initial wave amplitude to be incorporated into the regression equation. Consequently, the *NRMSE* for the density cases was reduced from 1.60

Table 6
Comparison of landslide parameters and depressed maximum wave amplitudes from previous studies(2,21) with predicted values.

Tag	V (m^3)	B (m)	D (m)	ρ (kg/m^3)	θ (°)	Observed η_{max} (m)	Predicted η_{max} (m)
R1	2.24×10^5	700	250	2000	22	3.0	2.7
R2	2.38×10^5	700	150	2000	25	2.0	5.9

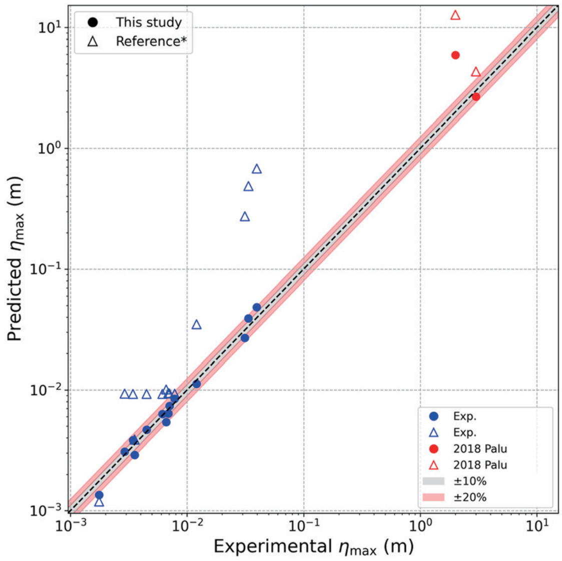

Fig. 6. (Color online) Comparison of predicted and observed wave amplitudes using the proposed scaling-based model, including laboratory measurements and field-reported tsunami amplitudes from the 2018 Palu.

to 0.23. These results indicate that landslide density is an important parameter for estimating the initial wave amplitude generated by SMFs and that considering its influence can improve predictive performance.

The proposed prediction equation is applicable within the parameter ranges considered in this study, including landslide densities of 1400–2800 kg/m^3 and slope angles of 22.5–67.5°. Furthermore, the applicable range of the proposed prediction equation can be further expanded by generating additional simulation data covering a wider range of landslide conditions and recalibrating the regression coefficients.

5. Conclusions

In this study, we simulated SMF-induced waveforms using a numerical model combining DualSPHysics and CHRONO and quantitatively evaluated the initial wave amplitude, which represents the maximum depression. A numerical sensing approach was employed to quantify the simulated water surface response. This model reproduced SMF movement and subsequent water surface fluctuation without relying on empirical coefficients, and its high reproducibility was confirmed through comparison with water-level measurements obtained using wave gauges in laboratory experiments.

On the basis of numerical simulation results, we reaffirmed that the initial wave amplitude is closely related to major landslide parameters. SMF volume and density were found to be most sensitive to amplitude variation. In particular, we observed that wave amplitude increased exponentially with decreasing initial submergence depth.

The proposed prediction equation demonstrated reasonable predictive performance not only in the laboratory but also in comparison with the 2018 Palu Bay tsunami, demonstrating overall improvements over existing empirical equations. Future work should expand the applicability of the prediction equation presented in this study through a wider range of field cases and additional wave flume experiments.

Acknowledgments

This work was performed under the auspices of the Ministry of Science and ICT (MSIT) of Korea (RS-2022-00144263).

References

1 D. R. Tappin, P. Watts, and S. T. Grilli: Nat. Hazards Earth Syst. Sci. **8** (2008) 243. https://doi.org/10.5194/nhess-8-243-2008
2 L. Schambach, S. T. Grilli, and D. R. Tappin: Front. Earth Sci. **8** (2021) 1. https://doi.org/10.3389/feart.2020.598839
3 P. Watts: Water Waves Generated by Underwater Landslides, Ph.D. Dissertation, California Institute of Technology (1997) p. 319.
4 F. Enet and S. T. Grilli: J. Waterw. Port Coastal Ocean Eng. **133** (2007) 442. https://doi.org/10.1061/(ASCE)0733-950X(2007)133:6(442)
5 R. Sabeti and M. Heidarzadeh: Landslides **19** (2022) 491. https://www.doi.org/10.1007/s10346-021-01747-w
6 A. Najafi-Jilani and B. Ataie-Ashtiani: Ocean Eng. **35** (2008) 545. https://doi.org/10.1016/j.oceaneng.2007.11.006
7 S. T. Grilli and P. Watts: Eng. Anal. Boundary Elem. **23** (1999) 645. https://doi.org/10.1016/S0955-7997(99)00021-1
8 S. T. Grilli and P. Watts: Proc. Int. Offshore and Polar Engineering Conf. (ISOPE, 2001) 1.
9 S. T. Grilli, S. Vogelmann, and P. Watts: Eng. Anal. Boundary Elem. **26** (2002) 301. https://doi.org/10.1016/S0955-7997(01)00113-8
10 S. T. Grilli and P. Watts: J. Waterw. Port Coastal Ocean Eng. **131** (2005) 283. https://doi.org/10.1061/(ASCE)0733-950X(2005)131:6(283)
11 P. Watts, S. T. Grilli, D. R. Tappin, and G. J. Fryer: J. Waterw. Port Coastal Ocean Eng. **131** (2005) 298. https://doi.org/10.1061/(ASCE)0733-950X(2005)131:6(298)
12 G. Zhang, J. Chen, Y. Qi, J. Li, and Q. Xu: Adv. Water Resour. **151** (2021) 1. https://doi.org/10.1016/j.advwatres.2021.103890
13 S. Viroulet, D. Cébron, O. Kimmoun, and C. Kharif: Geophys. J. Int. **193** (2013) 747. https://doi.org/10.1093/gji/ggs133
14 A. J. C. Crespo: DualSPHysics Wiki, GitHub https://github.com/DualSPHysics/DualSPHysics/wiki (accessed Jan. 2026).
15 A. J. C. Crespo, J. M. Dominguez, B. D. Rogers, M. Gómez-Gesteira, S. Longshaw, R. Canelas, R. Vacondio, A. Barreiro, and O. García-Feal: Comput. Phys. Commun. **187** (2015) 204. https://doi.org/10.1016/j.cpc.2014.10.004
16 M. Gómez-Gesteira, B. D. Rogers, A. J. C. Crespo, R. A. Dalrymple, M. Narayanaswamy, and J. M. Dominguez: Comput. Geosci. **48** (2012) 289. https://doi.org/10.1016/j.cageo.2012.02.029
17 J. M. Domínguez, G. Fourtakas, C. Altomare, R. B. Canelas, A. Tafuni, O. García-Feal, I. Martínez-Estévez, A. Mokos, R. Vacondio, A. J. C. Crespo, B. D. Rogers, P. K. Stansby, and M. Gómez-Gesteira: Comput. Part. Mech. **9** (2022) 867. https://doi.org/10.1007/s40571-021-00404-2
18 J. J. Monaghan: Annu. Rev. Astron. Astrophys. **30** (1992) 543. https://doi.org/10.1146/annurev.aa.30.090192.002551

19 J. J. Monaghan: J. Comput. Phys. **110** (1994) 399. https://doi.org/10.1006/jcph.1994.1034
20 A. J. C. Crespo, M. Gómez-Gesteira, and R. A. Dalrymple: Comput. Mater. Continua **5** (2007) 173. https://doi.org/10.3970/cmc.2007.005.173
21 W. Setyonegoro, M. Hanif, S. Khoiridah, M. Ramdhan, F. Fauzi, S. Karima, V. Isnaniawardhani, S. Pribadi, M. M. Muqqodas, P. Supendi, and S. Ardhyastuti: Kuwait J. Sci. **51** (2024) 1. https://doi.org/10.1016/j.kjs.2024.100245